Impact of Model Uncertainty Descriptions for High-Purity Distillation Control

The ways in which modeling uncertainties are described for a particular process critically affects the results obtained in robustness studies. In this paper, four multivariable robust stability methodologies are used to characterize and analyze the effects of model inaccuracy due to nonlinearity in high-purity distillation processes. The unstructured and structured singular value, numerical range, and a mapping of $\det(I + G_P G_c)$ are compared in terms of their ability to predict the stability of the dual-composition control system over a wide composition range. The importance of using uncertainty descriptions that include a realistic representation of the phase-magnitude relationship as well as the correlations between uncertainties in each element of the model is demonstrated. The conservatism associated with norm-bounded uncertainty descriptions reveals itself by the extent of detuning needed to insure stability and the subsequent degradation in control performance.

Karen A. McDonald
Ahmet Palazoglu
B. Wayne Bequette
Department of Chemical Engineering
University of California
Davis, CA 95616

Introduction

Control systems for chemical processes are typically designed using an approximate, linear, time-invariant model of the plant. The actual plant dynamics may differ from the nominal model due to many sources of uncertainty, such as nonlinearity, the selection of low-order models to represent a plant with inherently high-order dynamics, inaccurate identification of model parameters due to poor measurements or incomplete knowledge, and uncertainty in the manipulative variables and/or time-varying phenomena. In light of the differences between the actual plant and the nominal model, it is necessary to insure that the control system will be stable (and meet some predetermined performance criteria) when applied to the actual plant.

One of the most difficult steps in analyzing the robust stability and performance of any control system is the specification of an estimate of the uncertainty associated with the nominal process model. It is a critical step because an overestimation of the model inaccuracy will lead to excessively poor control performance and an underestimation may lead to instability. Several papers discuss ways in which model inaccuracy can be described and methods that can be used for assessing robust stability. The most common multivariable approaches that use singular values (Doyle and Stein, 1981; Arkun et al., 1984) and structured singular values (Doyle, 1982) assume that the actual plant can be described by a norm-bounded perturbation matrix in the frequency domain; Figure 1 shows a single-input/single-output (SISO) representation. The structured singular value (SSV) approach provides necessary and sufficient conditions for robust stability and performance for the situation in which uncertainty occurs simultaneously and independently in various parts of the overall control system (e.g., output and input uncertainty) but the perturbation matrix is still norm-bounded. Other approaches that do not require norm-bounded uncertainty descriptions are region mapping techniques, such as the methods used by Horowitz and Breiner (1981), Laughlin et al. (1986), and Saeki (1986), and the numerical range approach (Owens, 1984; Palazoglu, 1987). Horowitz uses arbitrarily shaped uncertainty regions on the complex plane to represent uncertain, nonlinear plants and presents a mapping technique to synthesize controllers. Laughlin utilizes a mapping technique to design SISO IMC controllers for systems characterized by arbitrary uncertainty sets. Saeki presents multivariable robust stability criteria for systems with arbitrarily shaped uncertainties. The numerical range approach introduces an effective way of expressing the magnitude-phase characteristics of the process perturbations.

In chemical process control, nonlinearity is one of the most significant sources of model inaccuracy. We usually have some knowledge about the structure of model inaccuracy due to non-

Correspondence concerning this paper may be addressed to K. A. McDonald or A. Palazoglu.
The current address of B.W. Bequette is Department of Chemical Engineering, Rensselaer Polytechnic Institute, Troy, NY 12181.

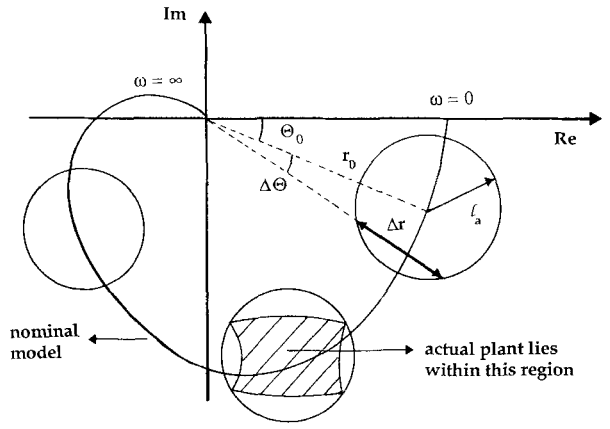

Figure 1. Norm-bounded uncertainty description for SISO system.

linearity, however, and this knowledge should be exploited in our robustness studies. In formulating the SSV problem, Doyle (1982) stresses the importance of using uncertainty descriptions that are physically based. This paper presents an example where the uncertainty is physically based and therefore indicates how well assumptions such as norm-bounded uncertainty descriptions represent the real process. In our analysis, we will characterize the model inaccuracy due to nonlinearity in high-purity distillation by considering a family of plants determined by linearizing a nonlinear model around different points in a given operating space. This approach, although approximate, is the only one feasible at the present, and can be used for any system if a nonlinear dynamic model is available that captures the essential nonlinear behavior of the process. Simplified models that predict gain and time constant changes as the process is perturbed over the expected operating regime can also be used to characterize the uncertainty. Several other researchers have used simple models, either empirical or physically based, to predict uncertainty due to nonlinearity in high-purity distillation towers. Morari and Doyle (1986) apply the SSV approach to analyze the robust stability and performance of high-purity distillation control with plant input (actuator) uncertainty. Skogestad and Morari (1987) present an SSV analysis for a high-purity distillation tower in which the uncertainty description (due to nonlinearity), although norm bounded, does reflect the correlations between elements of the transfer function matrix. Arkun and Morgan (1988) consider input, output, and additive uncertainties (norm bounded) simultaneously in their SSV analysis of moderate and high-purity distillation towers but do not consider uncertainty due to nonlinearity explicitly. Bequette et al. (1987) have applied the SSV approach to a distillation column with an intermediate condenser to design a robust nonsquare control system and compared conventional and material balance control structures.

Distillation Column Example

As an example, we consider dual-composition control using reflux and vapor boilup as manipulated variables in a high-purity distillation tower with the design specifications shown in Table 1. Although the nominal design point is $x_D = 0.994$, $x_B = 0.0062$, it is assumed that the tower may operate over an arbitrarily defined composition range $0.988 < x_D < 0.998$ and

Table 1. Distillation Tower Design Specifications

x_D	0.994
x_B	0.0062
x_F	0.50
n_T	40
n_S	20
α	1.386
β	0.02
F_0	10,000
L_0	61,909
V_0	66,908
M_{B0}	28,000
M_{c0}	28,000
M_{T0}	2,800

$0.002 < x_B < 0.012$. As a first approach, it is assumed that the nonlinear behavior of the tower can be represented by a simplified dynamic model for binary distillation (Luyben, 1973, pp. 148–151). Assumptions in this model include constant relative volatility, equimolar overflow, and 100% tray efficiency. Furthermore, we ignore level dynamics of the reboiler and condenser by assuming constant molar holdups and model the tray hydraulics with a linear relationship between the holdup and liquid flow from a tray. This model is linearized at various steady state operating points and the frequency response is numerically obtained using a stepping technique described by Luyben (1973).

Figure 2 presents the Nyquist plots for the nominal plant as well as the uncertainty sets obtained by linearizing the model over the entire operating regime at several frequencies. The solid lines in Figure 2 show the frequency response at the nominal design point for each element of the process transfer function matrix. These curves show that the composition responses of the high-order model can be adequately modeled as first order with only a small amount of dead time. When the model is linearized around other points in the operating range, different frequency responses are generated. The symbols shown in Figure 2 represent the uncertainty in the phase and magnitude for operation over the entire operating range ($0.988 < x_D < 0.998$, $0.002 < x_B < 0.012$) at a frequency of 0.001. Uncertainty sets at other frequencies can be generated in a similar manner.

Two important points can be made concerning the nature of these uncertainty regions. Although the shape of the region depends on the composition range selected, in general it will not be easily represented by a disk centered about the nominal point. Approximating the uncertainty by a norm bound introduces additional members of the uncertainty set that may not correspond to any physically possible plants (e.g., plants in the first quadrant for g_{11}). In addition, as shown in Figure 1, norm-bounded uncertainty representations specify a particular relationship between the uncertainty in the phase, $\Delta\theta$, and the magnitude, Δr at a particular frequency; that is,

$$\Delta r = \cos \Delta\theta \sqrt{(\ell_a(\omega) - r_0 \sin^2 \Delta\theta) + r_0 \sin^2 \Delta\theta} \qquad (1)$$

where $\ell_a(\omega)$ is the magnitude of the additive uncertainty and the radius of the bounding circle around the nominal plant at (r_0, θ_0). It can also be seen from Figure 1 that the uncertainty is not very well described by parametric uncertainty in the gains

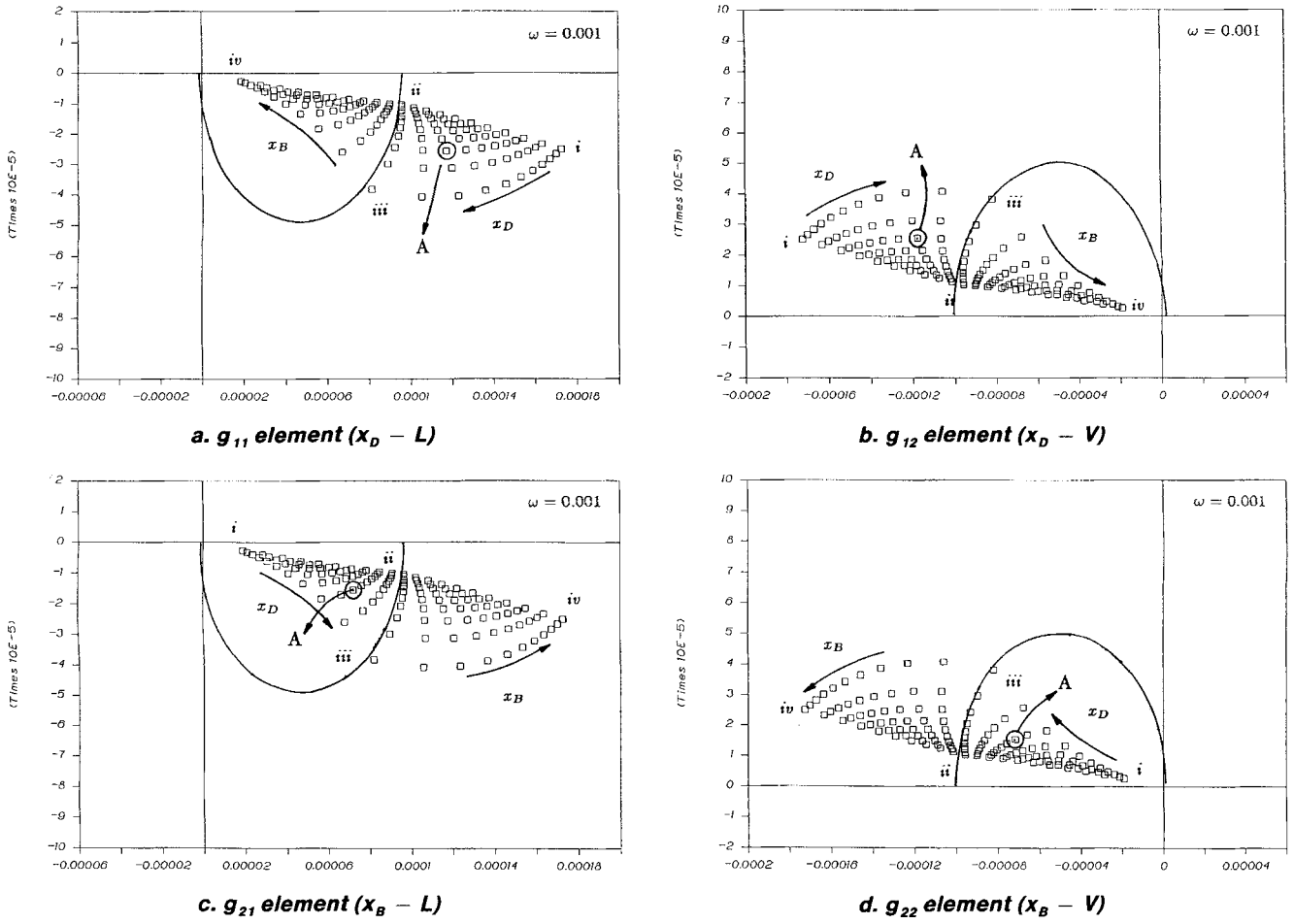

Figure 2. Nyquist plots for nominal (solid) and perturbed (symbols) plants at $\omega = 0.001$.

and the phases; that is,

$$g_{11_L}(\omega) < |g_{11}(j\omega)| < g_{11_H}(\omega) \tag{2}$$

$$\Delta\theta_{11_L}(\omega) < \angle g_{11}(j\omega) < \Delta\theta_{11_H}(\omega) \tag{3}$$

In addition to the particular phase-magnitude uncertainty structure associated with each element of the process matrix, there are also correlations between the uncertainties in the various elements. For example, point A on each of the plots, Figure 2a–d, corresponds to the same steady state operating point. Uncertainty descriptions that ignore the phase-magnitude structure or the correlations between elements will result in overly conservative results since many additional (and nonphysical) members of the uncertainty set are included in the analysis.

Based on the nominal model, a diagonal PI controller was designed to use as a basis of comparison for the different robust stability approaches. The controller is given by

$$G_c(s) = \begin{bmatrix} 450{,}000[1 + 1/(4.7s)] & 0 \\ 0 & -450{,}000[1 + 1/(4.7s)] \end{bmatrix} \tag{4}$$

The parameters were initially determined by using the Cohen-Coon tuning method for the nominal model ignoring interactions and subsequently detuned by trial and error.

In the next sections, we briefly review the robust stability analysis methods: the unstructured singular value, structured uncertainty, numerical range, and mapping techniques, and present the analysis results for the multiloop PI control structure using each of these approaches. It should be pointed out that all other uncertainties, other than nonlinearity, have been neglected in these analyses.

Robust Stability Analyses

Singular value analysis

For the closed-loop system in Figure 3, the stability and performance conditions depend on the variations of the actual plant transfer function, $G_p(s)$. Since these variations are not known exactly, the controller design has to be carried out in such a way as to guarantee the robustness of the system. Uusally, it is assumed that the discrepancy between a simple model of the process and the actual plant may be expressed through the output multiplicative uncertainty description (Doyle and Stein, 1981),

$$G_p(s) = [I + \Delta(s)]\, G_0(s) \tag{5}$$

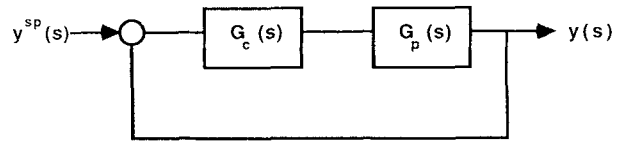

Figure 3. Feedback control system.

with the following information on the magnitude of $\Delta(s)$:

$$\|\Delta(j\omega)\|_2 = \sigma^*[\Delta(j\omega)] \leq \ell_m(\omega) \tag{6}$$

An estimate on the upper bound can be computed through the optimization formulation:

$$\ell_m(\omega) = \max_{\Delta \in \mathcal{D}} \sigma^*[G_p(j\omega)\, G_0(j\omega)^{-1} - I] \tag{7}$$

where the infinite set $\mathcal{D}$ represents the set of possible plant perturbations. Graphically, for a SISO system this can be interpreted as a band around the Nyquist plot of the nominal model with $\ell_m(\omega)$ being a factor of the radius of the circles at each frequency.

In this context, it is shown that the closed-loop system is robustly stable if (Doyle and Stein, 1981),

$$\sigma_*\{I + [G_0(j\omega)\, G_c(j\omega)]^{-1}\} \geq \ell_m(\omega) \tag{8}$$

for all frequencies. This condition establishes a multivariable stability margin that can be utilized to test the ability of a closed-loop system to handle process uncertainties with magnitudes as high as $\ell_m(\omega)$. It can also be interpreted as saying that large magnitudes of uncertainty can be handled by lowering the controller gains and thus decreasing the bandwidth of the system.

For the distillation column example, Eq. 8 is tested as shown in Figure 4. The magnitude of the uncertainty exceeds unity at steady state and at low frequencies. This is not unusual considering the highly nonlinear effect of product composition variations on the steady state gains. The robust stability criterion is violated and the indication is that the closed-loop system does not handle a process perturbation with the magnitude $\ell_m(\omega)$. In other words, one can find a particular realization of the plant satisfying Eq. 6 that would make the system unstable. Essentially, the singular value analysis is ineffective since, in this case, changing the controller parameters would not affect the steady state behavior of the quantity $\sigma_*[I + (G_0G_c)^{-1}]$. In conclusion, based on this analysis alone, robust stability of this process cannot be guaranteed for any set of plant perturbations described by Eq. 5 and 6. Naturally, while the magnitude bound is violated, one can still claim that the phase structure of this worst perturbation is such that it may not actually cause instability. Such a possibility however cannot be investigated using this unstructured singular value analysis.

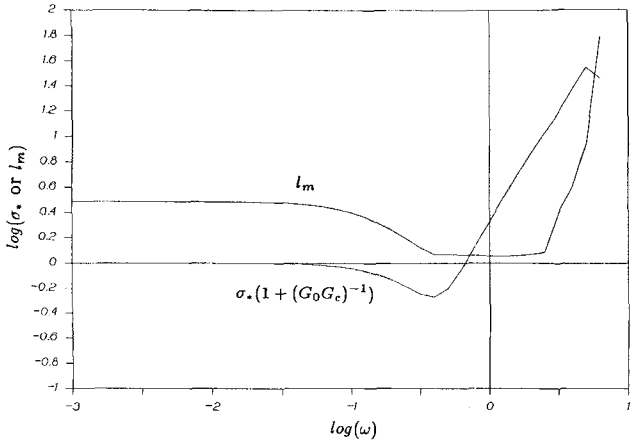

Figure 4. Singular value plot for distillation column example.

Structured uncertainty analysis

Singular value analysis is limited to systems that have an unstructured uncertainty representation, that is, the uncertainty is characterized by a single norm-bounded perturbation matrix. Doyle (1982) developed the structured singular value method to account for multiple or correlated perturbations in a process, allowing the uncertainty to be characterized by a block diagonal complex matrix $\Delta(j\omega)$, composed of m complex norm-bounded perturbation blocks $\Delta_i(j\omega)$ with $i = 1, 2, \ldots, m$.

The uncertainty due to process nonlinearities in a distillation column is highly structured, as can be seen from Figure 2. There is an obvious correlation in the perturbation in each of the gain elements, that is, the uncertainties in the transfer function elements g_{12}, g_{21}, and g_{22} are directly related to the uncertainty in g_{11}.

From Figure 2, it can be seen that the uncertainty may be characterized by an additive uncertainty representation where the actual process plant is described through the addition of a perturbation matrix with the nominal process:

$$G_p(j\omega) = G_o(j\omega) + \begin{bmatrix} \ell_a\Delta & -\ell_a\Delta \\ -\ell_a\Delta & \ell_a\Delta \end{bmatrix} \tag{9}$$

where Δ denotes a norm-bounded perturbation operator. Skogestad and Morari (1987) also utilize this perturbation form in their analysis of distillation column uncertainty. This is shown in Figure 5a in the context of a feedback control system. A similar system based on output multiplicative uncertainty is shown in Figure 5b. The weighting matrices (w_{1i} and w_{1o} for additive uncertainty and w_{2i} and w_{2o} for multiplicative uncertainty) are

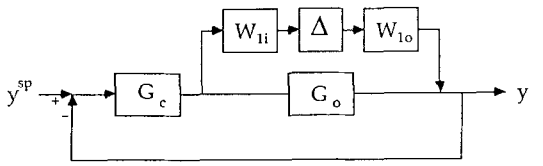

a. Additive uncertainty

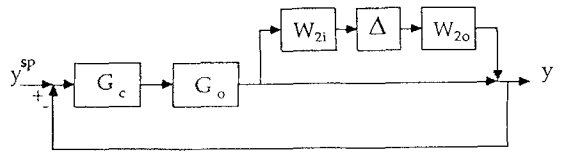

b. Output multiplicative uncertainty

Figure 5. Feedback structures for correlated uncertainty description.

Table 2. Weighting Matrices for System of Figure 5

Additive Uncertainty	Multiplicative Uncertainty
$w_{1i} = [1 \quad -1]$	$w_{2i} = [1 \quad -1]G_0(j\omega)^{-1}$
$w_{1o} = \begin{bmatrix} l_a(\omega) \\ -l_a(\omega) \end{bmatrix}$	$w_{2o} = \begin{bmatrix} l_a(\omega) \\ -l_a(\omega) \end{bmatrix}$

used to account for the structure of the uncertainty and are presented in Table 2. For the representation given by Equation 9, Δ becomes a scalar operator due to the particular correlation between the elements of the transfer function, with

$$|\Delta(j\omega)| \leq 1.0 \tag{10}$$

and l_a is the bound on the additive uncertainty:

$$l_a(\omega) = \max_{\Delta \in \mathcal{D}} |g_{p11}(j\omega) - g_{o11}(j\omega)| \tag{11}$$

Bequette et al. (1987) used a similar uncertainty description for a distillation column with an intermediate condenser.

Since all the uncertainty is described by a scalar perturbation, the robust stability condition reduces to

$$|w_{1i}G_c(I + G_oG_c)^{-1}w_{1o}| < 1.0 \tag{12}$$

Note that Eq. 12 is a simple method of calculation for $\mu(\omega)$ (Doyle, 1982) for the case of a scalar perturbation. This condition is also identical to the following test for multiplicative uncertainty:

$$|w_{2i}G_oG_c(I + G_oG_c)^{-1}w_{2o}| < 1.0 \tag{13}$$

The high degree of structure in the process uncertainty due to plant nonlinearity thus results in a simple robustness test. A plot of Eq. 12 is given in Figure 6, curve *A*, for the controller in Eq. 4. The robust stability condition is met at the low and high frequencies but fails in the mid-frequency region. However, after detuning these parameters to a significant degree ($K_1 = 196{,}000$, $K_2 = -196{,}000$, $\tau_1 = \tau_2 = 20$), we were able to satisfy Eq. 12, Figure 6, curve *B*. One can contrast these results with the unstructured singular value analysis results where the robust stability criteria were not met for any values of the controller parameters.

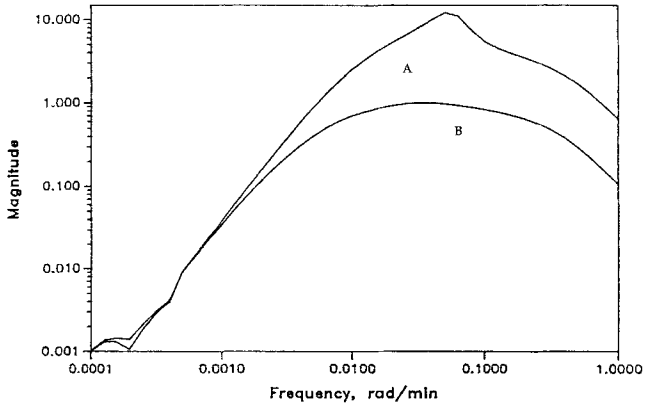

Figure 6. Structured uncertainty plot, Eq. 12.
***A*, controller parameters in Eq. 4**
***B*, detuned parameters $K_1 = 196{,}000$, $K_2 = -196{,}000$, $\tau_1 = \tau_2 = 20$**

Numerical range analysis

The numerical range of a matrix M is the set $V(M)$ of all complex numbers defined as the inner product $\langle x, Mx \rangle$ where x lies on the surface of a unit sphere such that $x^Hx = 1$. Some of the properties of the numerical range and methods of computation can be found in the literature (Halmos, 1982; Owens, 1984; Palazoglu, 1987). Typically, $V(M)$ represents a convex compact region in the complex plane that can be identified by its numerical radii and the phase angles, Figure 7. While the phases of the eigenvalues of M lie within the closed interval $[\theta_1, \theta_2]$, the gains of the eigenvalues lie within $[V_+, V_-]$. In short, the spectrum of M is contained within $V(M)$. This makes it an attractive tool to describe eigenvalue variations due to perturbations in the process. Specifically, the numerical range analog of Eq. 6 is given as

$$V[\Delta(\omega)] \subset \delta(\omega) \tag{14}$$

where the bounding set may be estimated as follows:

$$\delta(\omega) = \text{co}\{\bigcup_{\mathcal{D}} V[\Delta(\omega)]\} \tag{15}$$

This represents the union of all sets generated by the variation of $\Delta(\omega)$ in $\mathcal{D}$. In essence, $\delta(\omega)$ represents the designer's view of where the plant eigenvalues might lie. This region is also built as a convex set in the complex plane.

Within this setting, it is shown (Owens, 1984) that the closed-loop system in Figure 3 is robustly stable if,

$$(1 + V\{[G_0(\omega)G_c(\omega)]^{-1}\}) \cap -\delta(\omega) = \phi, \forall\, \omega \in \Omega \tag{16}$$

where ϕ stands for the empty set. This indicates that the set generated by the numerical range of the nominal model and the

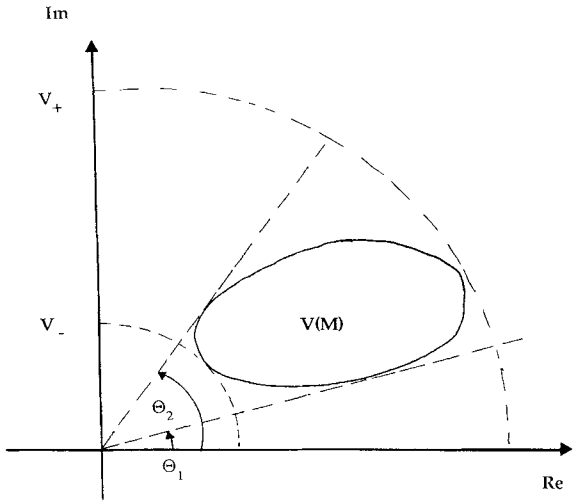

Figure 7. Typical representation of numerical range of a matrix.

controller has to avoid the model uncertainty set over the frequency range to guarantee robust stability. One now has the opportunity to tune the controllers and place the numerical range anywhere in the complex plane such that it does not intersect the region of uncertainty. This procedure does not necessarily generate "smaller" regions but implies that one can have "large" uncertainty and still have a robustly stable system as long as this region is conveniently placed away from the uncertainty. This effectively sets the stage for potential reduction of conservatism in robustness tests.

For the distillation column problem, the set $-\delta(\omega)$ is constructed by discretizing the set $\mathcal{D}$ using the 121 frequency points generated by the stepping technique described earlier. The convex closure of the union of all numerical ranges, Eq. 15, then gives the designer an idea about the region within which potential eigenvalue variations are expected, Figure 9. While this set is going to be used for robust stability analysis, it proves useful to briefly concentrate on the corner points of the uncertain region as given in Figure 2, and observe how these map into the complex plane through the numerical range operation. Figure 8 displays this mapping for four frequency points. One can now see the relative shapes of the numerical range associated with each of these perturbations and how they will contribute to the shape of $-\delta(\omega)$. Although the corner *ii* has a significant gain it will not play a role in the stability analysis since it is farther away from $(-1, 0)$ and the stability is going to be critical, especially for corners *i* and *iii* as they rotate in the complex plane as the frequency changes. These points correspond to cases where one of the products is becoming more pure and the other is becoming less pure. This gives one the opportunity to relate the numerical range predictions to the physical phenomena occurring in the system. This point will be further elaborated upon with the multivariable mapping approach.

When the expression $(1 + V\{[G_0(\omega)G_c(\omega)]^{-1}\})$ was first plotted using the controller parameters specified in Eq. 4, the two sets intersected around frequency $\omega = 0.1$. We had to detune the controllers to guarantee robust stability; we achieved this by keeping the proportional gains the same but increasing the time constants to 10.0 each. This yielded the desired result depicted in Figure 9. One can see that as $\omega \to 0$, both sets asymptotically approach (1, 0), never actually intersecting each other. Moreover, the sizes of the sets are essentially immaterial since they extend away from each other as frequency increases. In summary, the numerical range approach correctly identifies the magnitude-phase structure of the neglected nonlinearities and suggests a viable set of controller parameters. It has to be noted that the Eq. 16 is a sufficient condition and hence is subject to some degree of conservatism. Nevertheless, when the phase dependence of the uncertainty becomes critical, it does yield a reliable estimate of the robust stability of the feedback system.

Mapping analysis

Consider the case where n of the elements of the process transfer function matrix, G, and the controller transfer function matrix, G_c, have uncertainties associated with them, and denote these transfer functions as g_k for $k = 1, \ldots, n$. Suppose that the number of unstable poles of g_k is fixed (i.e., the number of unstable poles in the perturbed plant is the same as in the nominal plant). Further suppose that $g_k(j\omega)$ belongs to a closed set $U_k(\omega)$ where $U_k(\omega)$ denotes the inside of a polygon and $V_k(\omega)$ represents the set of vertices of U_k, Figure 10. By definition, the nominal plant $g_{k0}(j\omega)$ will also lie within $U_k(\omega)$.

Based on the multivariable Nyquist stability criterion it has been shown (Saeki, 1986) that the system will be asymptotically stable if and only if:

1. The system $(I + G_pG_c)^{-1}$ is asymptotically stable for the nominal values $g_k(s) = g_{k0}(s)$, and
2. The image of the Cartesian product of $U_k(\omega)$ under the mapping $\phi(g) = \det(I + G_pG_c)$ is simply connected and does not include zero for all ω

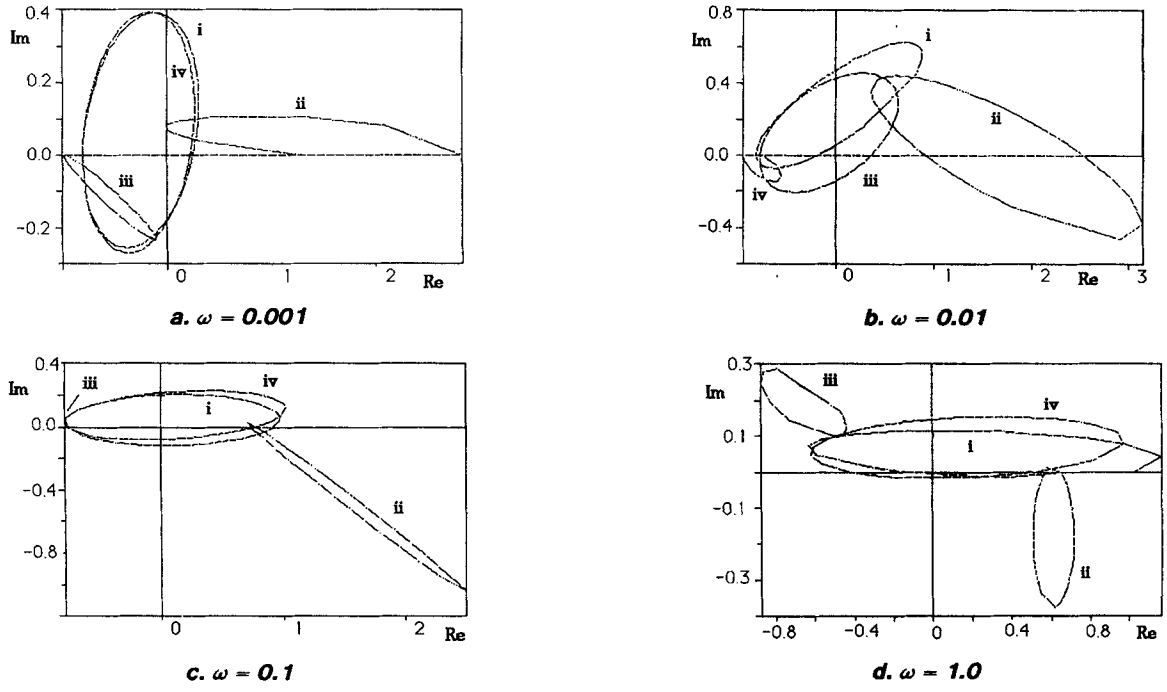

Figure 8. Numerical range mapping of four corner points of uncertainty region.

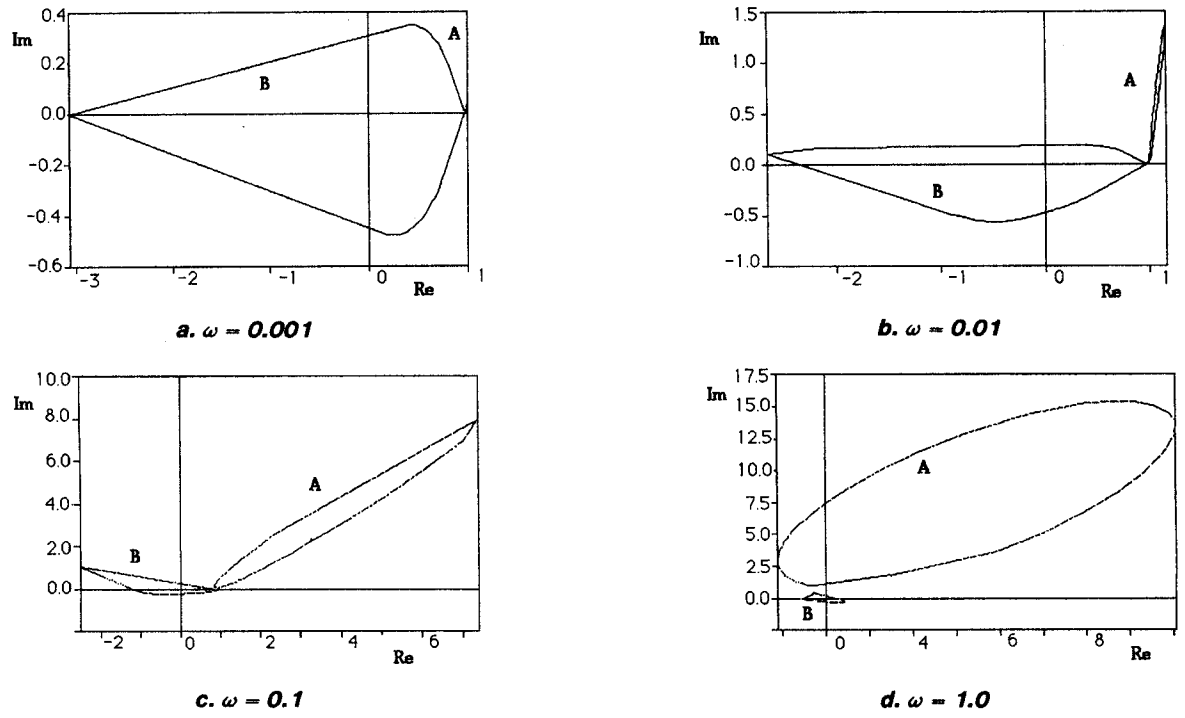

Figure 9. Robust stability test with numerical range approach.
A, set $(1 + V\{[G_0(\omega)G_c(\omega)]^{-1}\})$; B, set $-\delta(\omega)$

Furthermore, Saeki (1986) has shown that a sufficient condition for robust stability can be obtained by considering only the image of the Cartesian product of the vertices, $V_k(\omega)$, rather than the Cartesian product of the uncertainty sets $U_k(\omega)$. The system is asymptotically stable if

- Condition 1 above holds, and
- The convex closure of the image of the Cartesian product of V_k under the mapping $\phi(g) = \det(I + G_PG_c)$ does not include the origin for all ω

By definition, the Cartesian product includes all possible combinations of members from the different uncertainty sets. For the case of uncertainty due to nonlinearity, however, it does not make sense to map all possible combinations of members selected from each uncertainty set since the plants that are constructed in this manner do not correspond to any physical plant. As discussed in the Introduction, point A in the uncertainty set of g_{11} represents a particular steady state operating point (i.e., a particular x_D and x_B) that corresponds to the points labeled A in the uncertainty sets for the other elements of the process transfer function matrix. Instead of considering the image of the Cartesian product of the sets of vertices or the sets containing all members of the uncertainty regions, we therefore use only the plants comprised of members selected from the uncertainty region of each element that correspond to the same operating point. Since this domain is a subset of the Cartesian product, it is obvious that the convex closure of the mapping of the correlated set will be contained in the convex closure of the mapping of the Cartesian product, thus giving a less conservative result. Also, at each frequency this reduces the number of computations to m_k if vertices are used or the number of discretized points in the operating regime if the entire uncertainty set is considered.

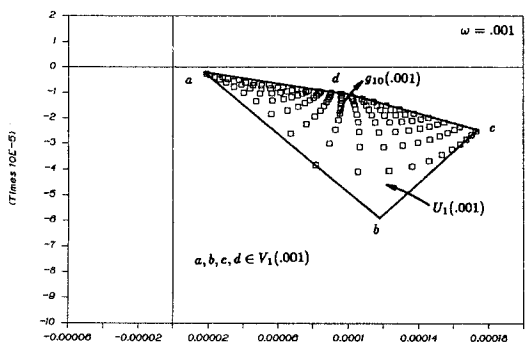

Figure 10. Uncertainty description in mapping approach.

Figure 11 shows the results of the least conservative mapping $\phi(g) = \det(I + G_PG_C)$ where G_p is composed of the corresponding points from the uncertainty families of each element of the process matrix, Figure 1, and the controller is given by Eq. 4.

If the Saeki mapping approach that is used involves the Cartesian product instead of the correlated uncertainty set, the mapping will be overly conservative. For example, Figure 12 shows the mapping using the Cartesian product of the sets of corner points corresponding to the four extremes in the composition range at a frequency of $\omega = 0.25$. The convex closure of this mapping includes the origin and therefore indicates that the system may be unstable.

The multivariable mapping technique is simple to use and can provide a more accurate analysis of robust stability when uncertainties (in either the process or the controller) display an arbitrary phase-magnitude relationship and correlations exist between uncertainties in transfer function elements, as is often the case for process nonlinearities.

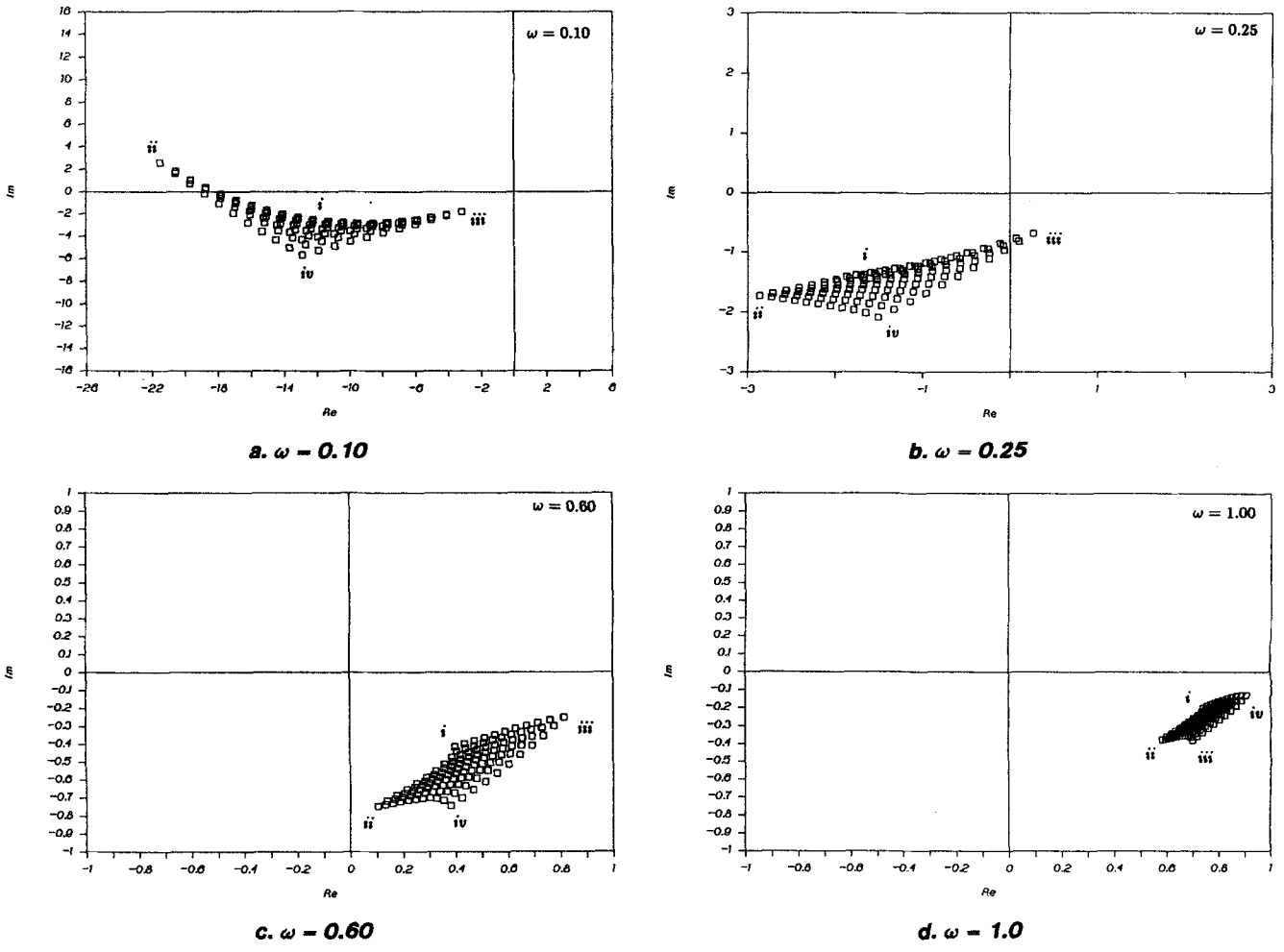

a. $\omega = 0.10$ b. $\omega = 0.25$ c. $\omega = 0.60$ d. $\omega = 1.0$

Figure 11. Mapping of det($I + G_pG_c$) at several frequencies.

Conclusions

The merits of four robust stability tests have been investigated for the case of high-purity distillation column control. The uncertainty due to sharp nonlinearities is shown to be well represented by numerical range and mapping approaches while the techniques based on norm-bounded uncertainty descriptions yield a highly conservative estimate of the region of uncertainty. For a particular controller, it has been shown that the singular-value-based robust stability tests were unable to detect the directionality of the uncertainty and gave conservative results.

The nonlinear dynamic model was also used to simulate set-point changes in the product compositions using the multiloop PI controller given by Eq. 4. Set-point changes were made in both product compositions simultaneously to determine the dynamic response when the tower is moved from the design point ($x_D = 0.994$, $x_B = 0.0062$) to any of the corner points of the operating space. As expected, the detuning of the controllers for the numerical range approach resulted in a slightly more sluggish response, with less overshoot and oscillations. Otherwise, the responses looked qualitatively similar to those obtained with the controller parameters in Eq. 4. On the other hand, the controller parameters that satisfied the structured uncertainty analysis yielded an extremely sluggish response, with long settling times that are practically unacceptable.

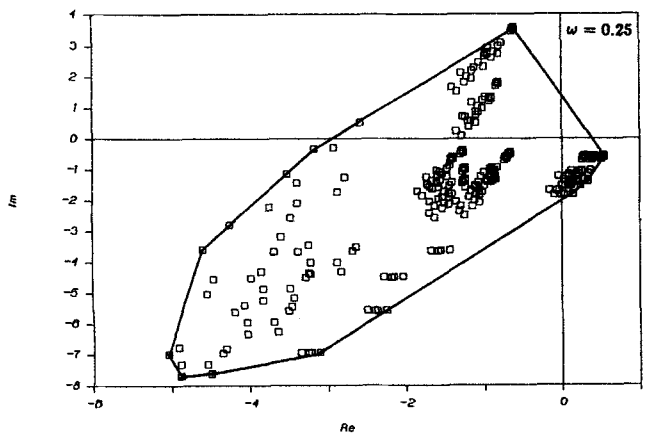

Figure 12. Mapping of det($I + G_pG_c$) using Cartesian product at $\omega = 0.25$.

Notation

co(·) = convex hull operator
$\mathcal{D}$ = set of possible plant perturbations
det(·) = determinant operator

F = molar feed flow rate, mol/min
g = element of a transfer function matrix
G = transfer function matrix
I = identity matrix
$j = \sqrt{-1}$
K = proportional gain
L = reflux rate, mol/min
ℓ_m = upper bound on magnitude of multiplicative uncertainty
ℓ_a = upper bound on magnitude of additive uncertainty
M = molar holdup, mol
n_T = total number of stages
n_S = number of stages in stripping section
r = magnitude
s = Laplace's variable
U_k = see Figure 10
$V(\cdot)$ = numerical range operator
V_k = see Figure 10
V = boilup rate, mol/min
x = product mole fraction

Greek letters

α = relative volatility
β = hydraulic constant
δ = region of eigenvalue variation, Eq. 15
Δ = perturbation matrix
μ = structured singular value
$\phi(\cdot)$ = uncertainty mapping defined by Saeki (1986)
σ = singular value
θ = phase angle
τ = integral time, min^{-1}
ω = frequency, rad/min

Subscripts

B = bottoms product
C = controller
D = distillate product
H = upper bound
L = lower
O = nominal model
P = actual plant
$*$ = minimum
$+$ = maximum
$-$ = minimum
1 = feedback loop between x_D and L
2 = feedback loop between x_B and V

Superscripts

H = complex conjugate
$*$ = maximum

Literature Cited

Arkun, Y., and C. O. Morgan III, "On the Use of the Structured Singular Value for Robustness Analysis of Distillation Column Control," *Comp. Chem. Eng.*, **12**, 303 (1988).

Arkun, Y., B. Manousiouthakis, and A. Palazoglu, "Robustness Analysis of Process Control Systems. A Case Study of Decoupling Control in Distillation," *Ind. Eng. Chem. Process Des. Dev.*, **23**, 93 (1984).

Bequette, B. W., R. R. Horton, and T. F. Edgar, "Resilient and Robust Control of an Energy-Integrated Distillation Column," *Proc. Am. Control Conf.*, 1027 (1987).

Doyle, J. C., "Analysis of Feedback Systems with Structured Uncertainties," *IEE Proc., Pt. D*, **129**, 242 (1982).

Doyle, J. C., and G. Stein, "Multivariable Feedback Design: Concepts for a Classical/Modern Synthesis," *IEEE Trans. Auto. Control*, **AC-26**, 4 (1981).

Halmos, P. R., *A Hilbert Space Problem Book*, Springer, New York (1982).

Horowitz, I., and M. Breiner, "Quantitative Synthesis of Feedback Systems with Uncertain Nonlinear Multivariable Plants," *Int. J. Systems Sci.*, **12**, 539 (1981).

Laughlin, D., K. G. Jordan, and M. Morari, "Internal Model Control and Process Uncertainty: Mapping Uncertainty Regions for SISO Controller Design," *Int. J. Control*, **44**, 1675 (1986).

Luyben, W. L., *Process Modeling, Simulation and Control for Chemical Engineers*, McGraw-Hill, New York (1973).

Morari, M., and J. C. Doyle, "A Unifying Framework for Control System Design Under Uncertainty and Its Implications for Chemical Process Control," *Chemical Process Control—CPC III*, M. Morari, T. J. McAvoy, eds., CACHE, Elsevier, New York (1986).

Owens, D. H., "The Numerical Range: A Tool for Robust Stability Studies?" *Sys. Control Lett.*, **5**, 153 (1984).

Palazoglu, A., "Robust Stability in IMC Framework Using the Numerical Range Approach," *Proc. Am. Control Conf.*, **1**, 643 (1987).

Saeki, M., "A Method of Robust Stability Analysis with Highly Structured Uncertainties," *IEEE Trans. Auto. Control*, **AC-31**, 935 (1986).

Skogestad, S., and M. Morari, "Design of Resilient Processing Plants. IX: Effect of Model Uncertainty on Dynamic Resilience," *Chem. Eng. Sci.*, **42**, 1765 (1987).

Manuscript received on Mar. 18, 1988 and revision received July 18, 1988.